Cross-section measurement and theoretical evaluation for the energy-transfer collision $Na(3P)+Na(3P)\rightarrow Na(4F)+Na(3S)$

M. Allegrini, C. Gabbanini, and L. Moi
Istituto di Fisica Atomica e Molecolare del Consiglio Nazionale delle Ricerche, Via del Giardino 7, I-56100 Pisa, Italy

R. Colle
Scuola Normale Superiore, Piazza dei Cavalieri 5, I-56100 Pisa, Italy

(Received 29 April 1985)

We have measured the cross section $\sigma(4F)$ for the collisional process $Na(3P)+Na(3P)\rightarrow Na(4F)+Na(3S)$. The experiment is based on the measurement of the intensities for $4F$, $4D$, and $3P$ fluorescence emissions in sodium vapor excited with a cw dye laser. $\sigma(4F)$ is determined relative to $\sigma(4D)$, which has been measured in an absolute way in previous experiments. Influence on $\sigma(4F)$ and $\sigma(4D)$ of the energy-transfer process $Na(4F)+Na(3S)\rightleftarrows Na(4D)+Na(3S)$ is also discussed. A theoretical evaluation of $\sigma(4F)$ and $\sigma(4D)$ relative to a chosen molecular channel is given and compared with the experimental determinations.

I. INTRODUCTION

Recently, there has been much interest in energy-transfer collisions (known also as energy-pooling collisions[1,2]) between two laser-excited $3P$ sodium atoms,

$$Na(3P)+Na(3P)\rightarrow Na(nL)+Na(3S)\ , \tag{1}$$

where nL indicates atomic levels lying higher than $3P$. Three of such nL states, namely $5S$, $4D$, and $4F$, are separated from the sum energy of two $3P$ atoms by a few kT (see Fig. 1). For the $5S$ and $4D$ levels there have been a number of experimental determinations of the cross section (updated results have been collected, for example, in Ref. 3). Here we report the first measurement of $\sigma(4F)$, the cross section for the population transfer to the $4F$ state, i.e., for the process

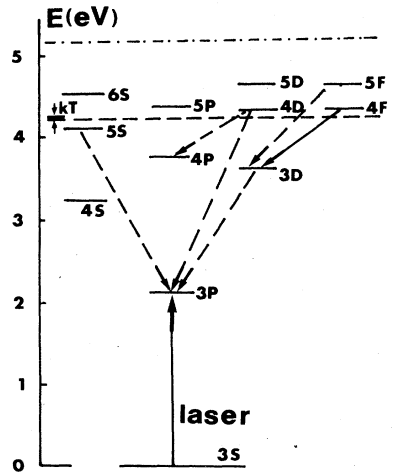

FIG. 1. Simplified energy-level diagram of atomic sodium. The dashed lines indicate the transitions of interest in this experiment and the horizontal line indicates the energy of two $3P$ atoms.

$$Na(3P)+Na(3P)\rightarrow Na(4F)+Na(3S)\ . \tag{2}$$

$\sigma(4F)$ was not measured previously because the $4F$-level fluorescence is in the near infrared, at 1.84 μm, outside the sensitivity of the apparatuses used for the determination of $\sigma(5S)$ and $\sigma(4D)$. The $4F$ state radiatively decays only to the $3D$ level and $\sigma(4F)$ could in principle be indirectly determined from the $3D$-level fluorescence intensity. However, since the $3D$ level is populated also through cascades from levels other than the $4F$, we prefer to modify the apparatus and perform a direct experiment. In this experiment we have also established the contribution of the collisional transfer process

$$Na(4D)+Na(3S)\underset{K}{\overset{K'}{\rightleftarrows}}Na(4F)+Na(3S)\ , \tag{3}$$

where K and K' are the rate coefficients of the reaction in the two directions. Process (3) is expected to be strong since the $4D$ and $4F$ levels lie very close in energy ($\Delta E=38\ cm^{-1}\approx 0.1kT$). However, our experiment has proved that the influence of process (3) on the energy-pooling cross sections $\sigma(4D)$ and $\sigma(4F)$ is only of the order of a few percent. This means that the values of $\sigma(4D)$ (Refs. 4 and 5) obtained in experiments which neglected process (3) remain correct.

To measure $\sigma(4F)$ we first tried the same approach and geometry as in our previous experiment[5] for the absolute determination of $\sigma(5S)$ and $\sigma(4D)$ involving excitation of sodium vapor from the ground state to the $3P$ state by means of a cw dye laser and measurement of the intensity ratio of $4F$-$3D$ to $3P$-$3S$ fluorescence. Unfortunately, the efficiency of the infrared detection apparatus is low compared to that of the visible apparatus and, as a consequence, the signal from the $4F$ level is weak compared to the fluorescence in the visible region of the spectrum from the $4D$ and $5S$ levels. We could easily increase the intensity of the $4F$-$3D$ fluorescence by increasing the laser power density and/or the atom density either by increasing the temperature of the cell or by adding a buffer gas

TABLE I. Fluoresence lines observed.

Transition	λ (μm)	Relative intensity[a] $T=260$°C (cell: no buffer gas)	$T=320$°C (cell: with buffer gas)
$4D$-$4P$	2.33	1.3	1.5
$4F$-$3D$	1.84	1	1
$4P$-$4S$	2.20	2.3	1.7
$4S$-$3P$	1.14	2.9	5.4
$5F$-$3D$	1.26		0.15
$6S$-$4P$	1.63		0.3
$7S$-$4P$	1.28		0.1

[a] The intensities are corrected for the apparatus response and they are normalized to the $4F$-$3D$ emission for each temperature.

(as will be shown later). However, one of our goals was to keep the laser power and the atom density at low values in order to avoid multiphoton and secondary collisional processes. So we took advantage of the fact that the $4D$ level has a fluorescence line, corresponding to the $4D$-$4P$ transition, in the near infrared (see Table I), in the same spectral region as the $4F$-$3D$ transition. By comparing the intensity of the $4D$-$4P$ line with the $4F$-$3D$ line we were able to measure $\sigma(4F)$ relative to the absolute value of $\sigma(4D)$ with an accuracy comparable to that of our previous experiment. In the same way we also determined an upper bound for $\sigma(5F)$.

From an experimental point of view the problems which led to large discrepancies in measured cross sections (see Table 1 of Ref. 3) have been overcome, while little work has been done from a theoretical point of view. The cross section of process (1) has been calculated only for the $4D$ state[6] by a procedure which does not use good-quality variational wave functions for the excited states and takes into account only the region of large interatomic distances. Here we report the first calculation for $\sigma(4F)$ and with the same approach we also find a value for $\sigma(4D)$ which is in better agreement with the experimental results. The method used and its results and limits will be described in detail in Sec. IV.

II. RATE EQUATIONS

The evolution of the population of the $4D$ and $4F$ levels, in the atomic system irradiated by the cw laser resonant with the $3S$-$3P$ transition, is affected by the energy-pooling collision process (1) and by the exchange process (3). In the conditions of our experiment, where the terms due to Penning ionization, electron collision ionization, and ionic recombination can be neglected, the rate equations have the form

$$\dot{N}(4F)=-A(4F,3D)N(4F)+N^2(3P)K(4F)+KNN(4D)-K'NN(4F)\ , \tag{4}$$

$$\dot{N}(4D)=-\sum_{nL}A(4D,nL)N(4D)+K(4D)N^2(3P)-KNN(4D)+K'NN(4F)\ , \tag{5}$$

where N is the atom density, $N(nL)$ is the population of the nL level, $A(nL,nL')$ is the spontaneous transition probability for $nL\rightarrow n'L'$, and $K(4F)$ and $K(4D)$ are the rate coefficients for the energy-pooling collisions. Since the collisions are thermal, $K(nL)=v\sigma(nL)$, where $v=\sqrt{8kT/\pi\mu}$ is the mean interatomic velocity. The rate coefficients K and K' for process (3) are connected by the detailed balance principle involving the level degeneracies as follows:[7]

$$K/K'=[g(4F)/g(4D)]\exp(-\Delta E/kT)\ .$$

At the temperature of our experiment $K/K'\simeq 1.26$. Solution of Eqs. (4) and (5) in the steady-state conditions yields the following relation for the population of the $4D$ and $4F$ levels:

$$\frac{N(4F)}{N(4D)}=\frac{[A(4D,3P)+A(4D,4P)+KN]K(4F)+KNK(4D)}{[A(4F,3D)+K'N]K(4D)+K'NK(4F)}\ . \tag{6}$$

by fitting the data to this expression both $K(4F)$ and K can be obtained.

Fluorescence from the $5F$ level has also been observed, under experimental conditions which will be described later. However, energy pooling is not the predominant process that populates the $5F$ level, which has an energy defect of 3150 cm^{-1}. Therefore, in the rate equations describing the population evolution of the $5F$ level, in addition to the radiative decay and

$$\mathrm{Na}(3P)+\mathrm{Na}(3P)\rightarrow\mathrm{Na}(5F)+\mathrm{Na}(3S)\ , \tag{7}$$

we must consider the following processes: electron-ion recombination, described by $K(R)$; radiative decay to the $5F$ state from upper levels; electron-impact ionization, described by $K(e)$; photoionization from the $5F$ level; Penning ionization, described by $K(3P,5F)$; associative ionization, described by $K(3S,5F)$; and electron-impact excitation of $5F$ from lower nL states, described by $K(e,nL)$. Taking all of these terms into account, the rate equation has the form

$$\dot{N}(5F) = -\sum_{nL} A(5F,nL)N(5F) + K(5F)N^2(3P) + K(R,5F)N^2(e) + \sum_{nL} K(e,nL)N(e)N(nL)$$
$$+ \sum_{n'L'} A(n'L',5F)N(n'L') - K(e,5F)N(e)N(5F) - B_i N(5F) I_L$$
$$- K(3P,5F)N(3P)N(5F) + K(3S,5F)N(3S)N(5F) \ . \tag{8}$$

In the photon ionization term $B_i I_L N(5F)$, I_L is the laser power density and $B_i = \sigma(PI)/h\nu_L$, with $\sigma(PI)$ the photoionization cross section and ν_L the laser frequency. The steady-state solution of Eq. (8) is

$$N(5F) = \frac{K(5F)N^2(3P) + K(R,5F)N^2(e) + \sum_{n'L'} A(n'L',5F)N(n',L') + \sum_{nL} K(e,nL)N(e)N(nL)}{\sum_{nL} A(5F,nL) + K(e,5F)N(e) + K(3P,5F)N(3P) + K(3S,5F)N(3S) + B_i I_L} \tag{9}$$

which suggests the possibility of obtaining $K(5F)$ by a procedure analogous to that used for the $4F$ level. However, it has been difficult to evaluate the influence on $K(5F)$ of the other terms and we have obtained only an upper limit to $K(5F)$ via the ratio $N(5F)/N(4F)$.

III. APPARATUS AND RESULTS

A sketch of the apparatus is shown in Fig. 2. An actively stabilized single-mode cw dye laser ($\Delta\nu \simeq 1$ MHz) excites sodium atoms to the $3P_{3/2}$ level with ~ 10 W/cm^2. The laser beam illuminates the sodium cell placed in a temperature-controlled oven; the temperature is varied between 235 °C and 310 °C. Since the cell is sealed and the vapor is saturated, the corresponding atomic density is conveniently determined from the Nesmeyanov tables[8] to be 10^{13}–10^{14} cm^{-3}. Two ordinary Pyrex cylindrical cells, prepared with standard vacuum techniques, have been used; one contains only sodium and the second contains sodium plus 10 Torr of He as buffer gas. The fluorescence is analyzed at right angles by a 0.35-m monochromator equipped with a 300-grooves/mm grating for the near infrared. The detector is a photoconductive PbS device sensitive to radiation in the (1–3)-μm region and cooled to dry-ice temperature for a better response. To improve the signal-to-noise ratio the laser beam is modulated at low frequency (481 Hz) by a mechanical chopper, and phase-sensitive detection is used. Typical fluorescence spectra recorded with this configuration are reported in Figs. 3(a) and 3(b).

As expected, the $4F$-$3D$ fluorescence intensity increases

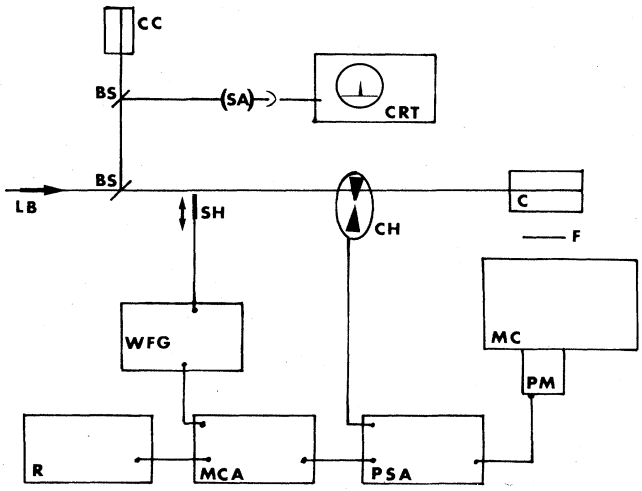

FIG. 2. Sketch of the experimental setup. LB, laser beam; BS, beam splitter; CC, control cell; SA, spectrum analyzer; CRT, cathode-ray tube; SH, shutter; CH, chopper; C, collision cell; F, filter; MC, monochromator; PM, photomultiplier; WFG, wave-function generator; R, recorder; MCA, multichannel analyzer; PSD, phase-sensitive detector (lock-in amplifier).

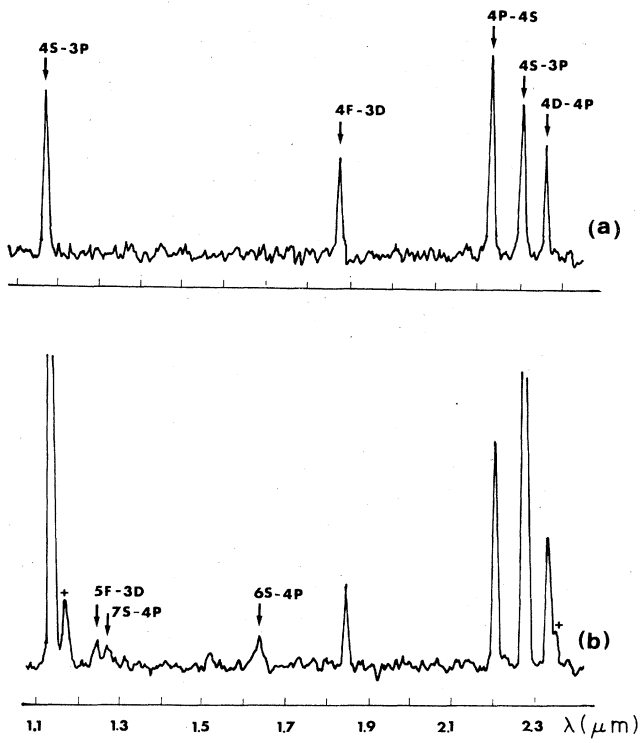

FIG. 3. Na fluorescence spectrum, uncorrected for the apparatus response. The laser power is ~ 100 mW; spectrum (a) is from a cell containing pure sodium at $T = 260$ °C while spectrum (b) is from a cell containing sodium at $T = 260$ °C plus 10 Torr of helium as buffer gas. The lines indicated with a + are due to potassium impurities in the cell.

dramatically with increasing temperature. However, this increase arises from contributions of processes other than energy pooling, processes which become important only at higher densities. In order to get a better signal-to-noise ratio at low temperatures, a further improvement of the apparatus was necessary. A second laser-beam chopper at a very low frequency (0.4 Hz) was used; a function generator drives this chopper and triggers a multichannel analyzer used for signal averaging. The statistical error is then reduced by the factor $1/\sqrt{N}$ where N is the number of averaging cycles of 5 sec duration each on the maximum of the fluorescence line. The signal is later on displayed on the analyzer and chart recorder.

The determination of $\sigma(4F)$ is obtained by observing the fluorescences $4F$-$3D$ at 1.84 μm and $4D$-$4P$ at 2.33 μm. It is sufficient to measure just the relative intensities because we only need the ratio $I(4F\text{-}3D)/I(4D\text{-}4P)$. In our experiment, laser intensity and fluorescence volume are the same for both $4F$ and $4D$ levels and radiation trapping is negligible for these high levels. In Fig. 4 the ratio of the two fluorescences of interest is plotted for a fixed temperature versus the laser power: It is clear that the variations are within 7%, which justifies our assumption. A first set of measurements was made with the cell containing pure sodium. The $4F$-$3D$ and $4D$-$4P$ fluorescences were recorded over $N=2^6$ averaging cycles on the multichannel analyzer so that the statistical error was decreased by the factor $1/2^3$. By using the relation between the transition probabilities and the line intensities (see, for example, Ref. 9) the $N(4F)/N(4D)$ ratio of Eq. (6) can be written in terms of the fluorescence line intensities. Data have been fitted to this expression and the resulting best-fit parameters are

$$K(4F)=(5.6\pm2.2)\times10^{-11}\ \mathrm{cm^3\,sec^{-1}}$$

and

$$K=(9.8\pm4.9)\times10^{-9}\ \mathrm{cm^3\,sec^{-1}}\ .$$

The best-fit curve for $\mathrm{Na}(4F)/\mathrm{Na}(4D)$ and the experimental values are reported versus temperature in Fig. 5.

The uncertainty in $K(4F)$ is slightly bigger than that in the absolute measurement of $K(5S)$ and $K(4D)$. The 50% indeterminacy of K shows that this experiment is not suitable for measuring the rate coefficient for the energy-transfer $4D$-$4F$ in sodium. If in the rate equations

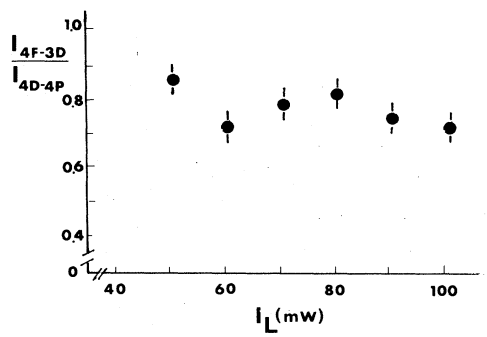

FIG. 4. Intensity ratio of the $4F$-$3D$ and $4D$-$4P$ fluorescences at $T=260\,^{\circ}\mathrm{C}$ vs laser power.

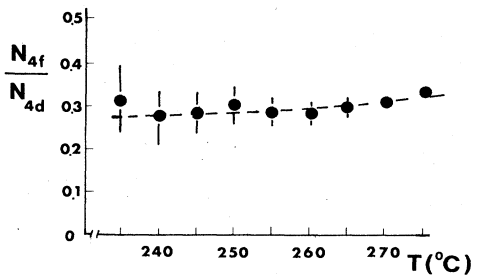

FIG. 5. Population ratio of the $4F$ and $4D$ levels. Dots represent the data and the dashed line the best-fit curve to Eq. (6).

(4) and (5) the term describing this transfer process is neglected and the data are fitted with the same procedure to the new expression for $N(4F)/N(4D)$, the result is

$$K(4F)=(6.0\pm2.4)\times10^{-11}\ \mathrm{cm^3\,sec^{-1}}\ .$$

Thus by neglecting the exchange $4D$-$4F$ process (3) the relative error introduced in the energy-pooling cross section $\sigma(4F)$ is only of order 5%, at least at the temperatures of our experiment. Since $\sigma(4D)$ is about one order of magnitude bigger than $\sigma(4F)$ the influence of the $4D$-$4F$ collisions (which were indeed neglected in both the experiments of Refs. 4 and 5) is even less important for the determination of $\sigma(4D)$.

As shown in Fig. 3(b) the emission spectrum recorded with a cell containing sodium plus a buffer gas also contains fluorescence lines originating from the $5F$, $6S$, and $7S$ levels. (For comparison, all observed lines are listed in Table I.) The presence of lines from such high states clearly shows that the buffer gas favors, in addition to energy pooling, other collisional processes. Earlier experiments in which visible fluorescence spectra resulting from laser irradiation of sodium vapor were obtained also showed that atomic levels lying higher than the $3P+3P$ energy were produced.[10] The precise sequence of reac-

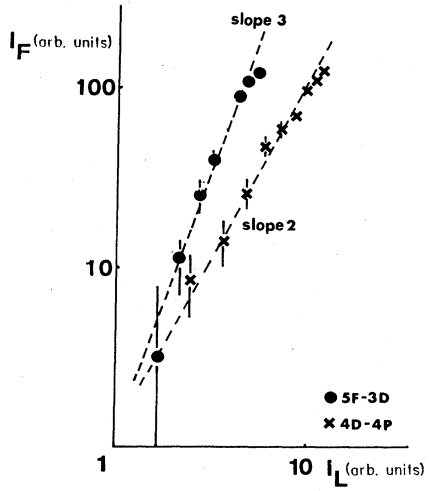

FIG. 6. Log plot of the fluorescence intensity for transitions from the $5F$ and $4D$ levels vs laser intensity.

tions that leads to the production of these states is quite complicated, involving superelastic electron collisions, secondary collisions of the atoms excited by primary energy pooling, and ionization mechanisms with subsequent electron-ion recombination. In this work we will concentrate only on the population mechanism of the $5F$ level. The dependence upon the laser power of the $5F$-$3D$ fluorescence intensity, compared to the $4F$-$3D$ line (see Fig. 6), gives direct evidence that the $5F$ and $4F$ levels are populated through different mechanisms. From our experiment it is not possible to determine the contribution to the population of the $5F$ level of each process taken into account in the rate equation (8). However, since in the full range of temperatures of our experiments emission from the $5F$ level has not been observed in the cell without buffer gas, we are able to place an upper limit on the cross section $\sigma(5F)$ of process (7). Measurement of the intensity of the $5F$-$3D$ line leads for this limit to $K(5F) < 10^{-13}$ cm sec^{-1}.

IV. THEORETICAL APPROACH

In this section a theoretical evaluation of the cross sections for the energy-transfer collisions (1) with $nL = 4D$ and $4F$ is given. To our knowledge this is the first calculation for $\sigma(4F)$, and the result is in good agreement with the measured value reported in Sec. III. For $\sigma(4D)$ we find a value that agrees better than other theoretical calculations[6] with the results of reliable experiments.[4,5]

The population of the highly excited atomic levels, due to energy-transfer collisions, can be looked at as resulting from transitions among different electronic molecular states connected to various dissociation limits and coupled by the total Hamiltonian. In our experiment the total averaged cross section is measured for a given set of initial and final atomic states; no other information is available about the collision process itself. Therefore, for a quantitative comparison between the theoretical predictions and the experimental results one should in principle include all the possible electronic states that dissociate into the product of the collisional process and solve the complete set of coupled equations for each possible value of the relative velocity and of the total angular momentum. The resulting values of σ should be averaged with statistical weights which depend on the distribution of the atomic fragments among the initial states.

In our specific case the classification of the electronic molecular states according to the projection Λ of the electronic angular momentum along the internuclear axis gives this set of initial states, connected to the $(3P+3P)$ dissociation limit,

$$({}^1\Sigma_g^+(2), {}^3\Sigma_g^-, {}^1\Pi_g, {}^3\Pi_g, {}^1\Delta_g)\,,$$
$$({}^3\Sigma_u^+(2), {}^1\Sigma_u^-, {}^3\Pi_u, {}^1\Pi_u, {}^3\Delta_u)\,, \tag{10}$$

and this set of final states, connected to the $(3S+4D)$ and $(3S+4F)$ dissociation limits,

$$({}^1\Sigma_{g/u}^+, {}^3\Sigma_{g/u}^+, {}^1\Pi_{g/u}, {}^3\Pi_{g/u}, {}^1\Delta_{g/u}, {}^3\Delta_{g/u})\,, \tag{11}$$

plus $({}^1\Phi_{g/u}, {}^3\Phi_{g/u})$ for the $(3S+4F)$ limit. Almost every pair of states having the same g/u and $+/-$ symmetry is coupled by some terms in the Hamiltonian: the derivatives of the radial internuclear distance for states with the same Λ and S, the Coriolis terms for states having the same S but $\Delta\Lambda = \pm 1$, the spin-orbit operator for states with different values of S, etc. Thus a complete *a priori* treatment of this problem is quite impractical considering also that the molecular states involved in this problem are highly excited electronic states. However, for obtaining an order of magnitude of the measured cross section and taking into account that we are dealing with slow (thermal) collisions, we have selected among all the states given in (10) one energetically favorable entry channel, that represented by the ${}^1\Sigma_g^+$ molecular states, and we have calculated the contributions to the measured cross section due to the transitions from these states to the other ${}^1\Sigma_g^+$ states that go to the $(3S+nL)$ dissociation limits. Because of the slow-velocity regime and since large interatomic distances ($R > 20$ a.u.) are important in the collisions between our excited atoms, it seems reasonable to disregard the centrifugal coupling with the Π states. Also, neglect of the spin-orbit coupling does not represent a crucial approximation in the case of sodium atoms. For these reasons we believe that significant comparisons can be made between the cross sections for the transition processes $(3P+3P) \rightarrow (3S+4D,\ 3S+4F)$ calculated using the subset of the ${}^1\Sigma_g^+$ electronic states and the experimental results valid at least as to order of magnitude.

In the following we describe briefly the method used to construct the electronic wave functions and to calculate the potential-energy curves as well as the coupling matrix elements between these wave functions. Finally, we describe the semiclassical procedure for evaluating the cross section for the $3P+3P$ collisions which populate the $4D$ and $4F$ levels, and we compare our results with the measured values.

A. Wave functions and electronic terms

We start from the solution of the electronic problem for the two separated atomic fragments. For each of them we construct a set of Hartree-Fock orbitals separately optimized for the various states, starting from the ground up to the $(4d)$ and $(4f)$ excited ones. Note that from now on we will identify each atomic state by using the quantum numbers n and l (lower case) of its valence electron in the independent particle description. The Hartree-Fock orbitals are used for constructing valence-bond wave functions, having ${}^1\Sigma_g^+$ symmetry and corresponding to the various dissociation limits of the Na_2 molecule: $(3s,nl)$ with $n=3$, 4, and 5; $l=0$, 1, 2, and 3; and $(3p,3p)$. Writing each electronic wave function as an antisymmetrized product of group functions, we give to each molecular state the representation

$$\psi(1',2',\ldots,N',1'',2'',\ldots,N'';1,2) = M\hat{A}[\Phi_{CA}(1',2',\ldots,N') \times \Phi_{CB}(1'',2'',\ldots,N'')\Phi_V(1,2)]\,, \tag{12}$$

where Φ_{CA} is the group function for the singlet ground state of the core electrons of the atom A having the fol-

lowing structure in terms of the atomic core orbital centered on A:

$$\Phi_{CA} = | \, 1s_A \overline{1s}_A 2s_A \overline{2s}_A 2p_{ZA} \overline{2p}_{ZA} 2p_{YA} \overline{2p}_{YA} 2p_{XA} \overline{2p}_{XA} \, | \ . \tag{13}$$

Analogously, Φ_{CB} in (12) describes the core electrons of the atom B while Φ_V is the group function for the valence electrons in the $^1\Sigma_g^+$ state with the following valence-bond structure [corresponding to the $(nl)(n'l')$ dissociation limit]:

$$\Phi_V(1,2) = \tfrac{1}{2} M_V (1+\hat{i})(1+\hat{\mathscr{P}}) \phi_{nl_A}(1) \phi_{n'l'_B}(2) \frac{\alpha\beta - \beta\alpha}{\sqrt{2}} \ , \tag{14}$$

where α and β are the usual spin functions.

We notice that in (12) $\hat{A}$ is the total antisymmetrizer and in (14) M_V is a normalization constant, while $\hat{i}$ and $\hat{\mathscr{P}}$ are, respectively, the inversion and the permutation operators acting on the spatial electronic coordinates. We construct a set of such $^1\Sigma_g^+$ electronic molecular functions, starting from the lowest dissociation limit $(3s+3s)$ up to the $(3s+4f)$ one. At infinite internuclear distance these wave functions $\{\psi\}$ are automatically orthogonal, as are the orbitals used for their construction. Going to finite internuclear distances and keeping the same structure (14) for each valence group function, we allow free overlap between the two valence orbitals of each Φ_V, while orthogonalizing them to the core orbitals and the core orbitals among themselves for each ψ. In such a way and without introducing any other configuration we can take into account the contributions due to the so-called ionic structures, which are essential for a complete description of the state, and we can also disregard the corrections due to the basis superposition errors.[11]

Following such a procedure we obtain at each internuclear distance a set of electronic wave functions that are weakly dependent on the internuclear distance because of their structure and whose orbitals maintain a well-defined atomic character. Such functions are coupled in practice only by the electronic Hamiltonian and can cross each other at finite internuclear distance: They therefore represent our diabatic reference states. Note that these wave functions are in general mutually nonorthogonal, but they can be easily orthogonalized without changing their main characteristics using the Löwdin procedure:[12]

$$\{\psi'\} = \{\psi\} \underline{A}^{-1/2} \ , \tag{15}$$

where $\underline{A}$ is the overlap matrix among $\{\psi\}$. The behavior of the potential-energy curves, obtained from $\{\psi'\}$, is shown in Fig. 7 for the states of interest.

This diabatic representation has a physical meaning at sufficiently large internuclear distances, where the Hund (d) coupling case is appropriate, while at smaller internuclear distances ($R < 20$ a.u.) the interatomic potential strongly mixes the atomic symmetries and an adiabatic representation becomes more physically significant. This change of representation can be readily achieved by diagonalizing the matrix representative of the electronic Hamiltonian in the diabatic basis set: The eigenvalues of

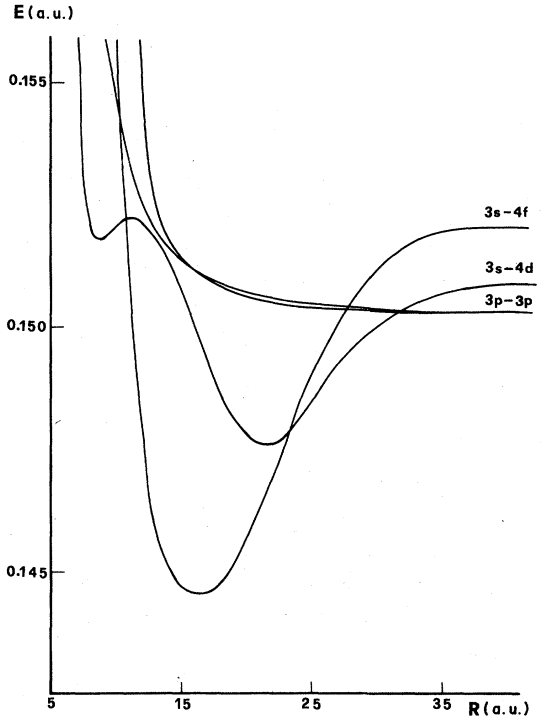

FIG. 7. Behavior with the internuclear distance R, given in atomic units (a.u.), of the four diabatic $^1\Sigma_g^+$ terms going to the $(3p+3p)$ and $(3s+4d)$,$(3s+4f)$ dissociation limits. The energies are given in a.u. with respect to the $(3s+3s)$ dissociation limit.

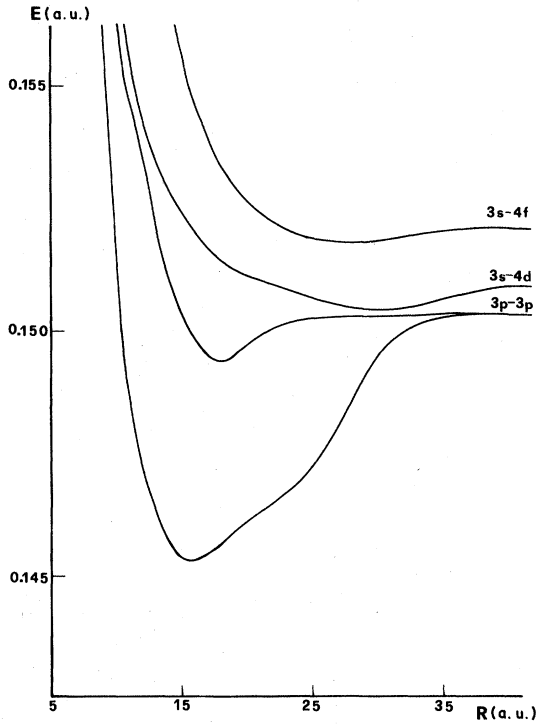

FIG. 8. Behavior with the internuclear distance R, given in atomic units (a.u.), of the four adiabatic $^1\Sigma_g^+$ terms going to the $(3p+3p)$ and $(3s+4d)$,$(3s+4f)$ dissociation limits. The energies are given in a.u. with respect to the $(3s+3s)$ dissociation limit.

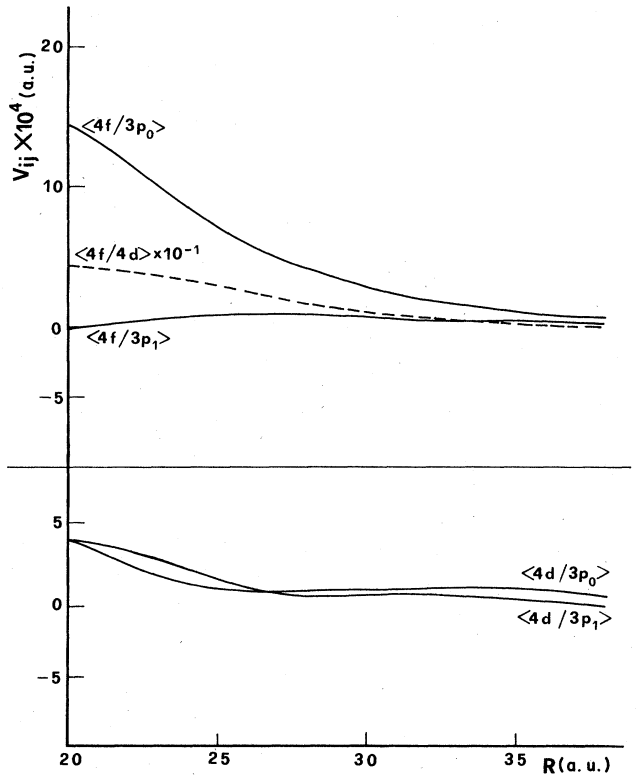

FIG. 9. Behavior with the internuclear distance R, given in atomic units (a.u.), of the coupling terms V_{ij}, given in a.u., between the various diabatic states of interest. The two $^1\Sigma_g^+$ states going to the $(3p+3p)$ dissociation limit are classified as $3P_0$ (the one higher in energy) and $3P_1$ (the lower one).

this matrix represent the adiabatic terms whose behavior as a function of the internuclear distance is shown in Fig. 8 for the states of interest. The eigenvectors give the expansion coefficients of the adiabatic many-determinant wave functions that are the solutions of the electronic problem for the various molecular states. These adiabatic wave functions are coupled by the radial derivatives of the internuclear distance whose matrix elements become relevant and change rapidly at the crossing points between the diabatic states.

In the following cross-section calculations we have utilized the adiabatic surfaces for treating the nuclear dynamic and the diabatic terms and wave functions to locate the transition points between the various surfaces and for evaluating the transition probabilities at internuclear distances $R \geq 20$ a.u. The behaviors of the coupling matrix elements between the diabatic states of interest are shown in Fig. 9.

Finally, we observe that from our variational calculations we get many-determinant wave functions for the valence electrons moving in an effective potential due to core electrons, which are described by the same Hartree-Fock single-determinant wave function for each state. The differences between the calculated and the experimental values of the energy defects between the various dissociation products are essentially due to the fact that we disregard the core-valence correlation energy and polarization effects which, however, should not influence to any large extent the coupling matrix elements between the various wave functions.

B. Cross sections

The calculation of the cross sections for the energy-transfer collisions (1) with $nl=4d$ and $4f$ has been carried out in a semiclassical way as a four-state problem involving the two $^1\Sigma_g^+$ adiabatic states that go to the $(3p+3p)$ dissociation limit and the two adiabatic states going to the $(3s+4d)$ and $(3s+4f)$ limits.

Following an approach suggested in Refs. 13 and 14 we have treated the four-state interaction as a sequence of two-state interactions by assuming that each transition between adiabatic curves is localized at their complex intersection point, with a local probability independent of all the other curves. Such an approach disregards second-order effects due to the interference with the other states, but the results are usually in excellent agreement with accurate quantum calculations.[14] The method used for the cross-section calculations is sketched in what follows.

The total cross section for an inelastic process connecting the (λ) and (μ) states depends on the square modulus of the (μ,λ) element of the S matrix, which can be written as

$$S_{\mu\lambda}=\sum_n P_n e^{i\varphi_n} . \tag{16}$$

In (16) the sum runs over all the classical trajectories starting on the curve (λ) and ending on curve (μ), while P_m is the product of all the probability factors for making or not a transition at each branch point of that trajectory and φ_n is the real phase accumulated along that trajectory. Looking at the scattering process as a series of local transitions between pairs of states, we can write the scattering matrix as a product of propagators along the adiabatic curves and propagators for each branch point of the trajectory. The matrix representation of the propagator along the internuclear coordinate from R_1 to R_2 in a region devoid of the intersection points is given by a diagonal matrix, whose jth element corresponding to the adiabatic curve $W_j(R)$ is

$$F_j^{\mp}(R_1,R_2)=\exp\left[\mp i\int_{R_1}^{R_2} k_j(R)dR\right] , \tag{17}$$

where $K_j(R)=\{2m[E-W_j(R)]\}^{1/2}$ and the upper (lower) sign corresponds to the incoming (outgoing) part of the trajectory. On the other hand, the matrix representation of the local propagator around the complex intersection point, for example, of W_1 and W_2, is given by

$$G_{1,2}^{\mp}=\begin{bmatrix} (1-p)^{1/2} & \mp p^{1/2}e^{\mp i\chi} & 0 & 0 \\ \pm p^{1/2}e^{\pm i\chi} & (1-p)^{1/2} & 0 & 0 \\ 0 & 0 & 1 & 0 \\ 0 & 0 & 0 & 1 \end{bmatrix} , \tag{18}$$

where p gives the transition probability from the adiabatic curve W_1 to the adiabatic curve W_2 and χ is a phase whose magnitude depends on the coupling strength be-

tween the two states.

Since in our problem the intersection points between the diabatic curves are well separated both reciprocally and with respect to the classical turning points, and furthermore, the diabatic curves are sufficiently linear and their coupling terms quite constant near the crossing points, we have used the Landau-Zener approximation for evaluating the transition probability p and the phase factor in (18). Thus we get

$$p=\exp\left[\frac{-2\pi\,|\,V_{12}(R_x)\,|^2}{v_0\left|\frac{d}{dR}[V_1(R)-V_2(R)]\right|_{R=R_x}}\right], \tag{19}$$

$$\chi=\tfrac{1}{4}\pi\,, \tag{20}$$

where $V_1(R)$ and $V_2(R)$ are the diabatic terms which cross each other at $R=R_x$ and are coupled by $V_{12}(R)$, while $v_0=(1/2m)(K_1+K_2)\,|_{R=R_x}$ is the local velocity of the nuclear motion at R_x. In our calculations we have used the adiabatic curves shown in Fig. 8, implemented by the introduction of the centrifugal potential, and the intersection points between each pair of diabatic curves V_i and V_j have been derived from Fig. 7 and the coupling terms V_{ij} from Fig. 9. Finally, every element $S_{\mu\lambda}$ of the scattering matrix has been calculated as the product of the appropriate propagators for the ingoing and outgoing parts of the trajectory, with the proper boundary conditions imposed for the vanishing of the wave functions at each classical turning point.

The total cross section for the transition process $(\lambda\rightarrow\mu)$ has been calculated by integration of $|\,S_{\mu\lambda}\,|^2$ over the impact parameter and the result has been averaged over a Maxwellian distribution $f(v,T)$ of the relative velocity v of the atoms at various given temperatures T, according to the expression

$$\sigma_{\mu\leftarrow\lambda}(T)=2\pi\int_{v_{\min}}^{v_\infty} f(v,T)dv\int_0^{b_{\max}}|\,S_{\mu\lambda}(b,v)\,|^2 b\,db\,. \tag{21}$$

In (21), $v_{\min}$ represents the minimum relative velocity for covering the energy defect between the final and initial states and $b_{\max}$ the largest impact parameter for which the incoming particle can surmount the effective potential at the crossing point. Note that the presence of the centrifugal barrier is taken into account by a proper definition of $b_{\max}$,[15] which reduces the range of the integration over the impact parameter when the maximum of the centrifugal barrier lies outside the crossing points between two surfaces, thus practically eliminating problems arising from coalescence of the paths.

In Table II we report the results of our calculations of $\sigma(3p\rightarrow 4d)$ and $\sigma(3p\rightarrow 4f)$ for the two entry channels and the average of these values for each transition process, at $T=500$ K, which is a value intermediate between the experimental ones. As can be seen from Table II, the order of magnitude of the calculated cross sections coincides with the experimental values for both $\sigma(4D)$ and $\sigma(4F)$ and, furthermore, the value of $\sigma(4F)$ lies within the range of the experimental error. Note that this calculation, unlike previous ones,[6] exploits the entire adiabatic energy surfaces for evaluating the cross sections, taking into account the interference effects between the various wave functions which have been derived variationally. More accurate predictions of the experimental results can be obtained by considering other electronic states both as entry channels for the collision and in the expansion of the total wave function and by evaluating completely the correlation and polarization contributions for the various electronic terms.

V. CONCLUSIONS

A simple modification of the apparatus used for measurements of the energy-transfer cross sections in collisions between two $3P$ sodium atoms has allowed the direct observation of the population transfer to the $4F$ and $5F$ levels. Working in an atom density range where other processes should be negligible we have established that energy-pooling collisions are indeed the dominant mechanism which populates the $4F$ level and we have measured the relative cross section. A theoretical model based on the construction of the molecular potential curves connected to the atomic fragments involved in the collision has been developed. The cross section calculated considering the contribution only from the $^1\Sigma_g^+$ molecular states is in good agreement with the measured result.

With the same theoretical approach the cross section

TABLE II. Comparison between our experimental and theoretical determinations of the $4D$ and $4F$ energy-pooling cross sections. The states $(^1\Sigma_g^+)_1$ and $(^1\Sigma_g^+)_2$ refer, respectively, to the energetically lower and higher entry channels, and $\langle\sigma\rangle$ is the mean value of their contributions to the total cross section which must be compared with the experimental result.

	$\sigma(4D)$ (cm^2)	$\sigma(4F)$ (cm^2)	T (K)
Expt.	$(3.2\pm1.1)\times10^{-15}$		483
		$(5.7\pm2.3)\times10^{-16}$	523
Calc.: $\langle\sigma\rangle$	1.0×10^{-15}	6.8×10^{-16}	500
$(^1\Sigma_g^+)_1$	9.4×10^{-16}	3.5×10^{-16}	500
$(^1\Sigma_g^+)_2$	1.1×10^{-15}	1.0×10^{-15}	500

for the $4D$ state has also been evaluated. This result is slightly outside our measurement reported in a previous work.[5] We do not have a clear explanation for this fact; however, we note that the experiment was performed at $T=487$ K while the calculation was carried out at $T=500$ K. $\sigma(4D)$ apparently decreases with temperature and indeed the experimental value of Huennekens and Gallagher[4] obtained at $T=597$ K is closer to the theoretical evaluation.

ACKNOWLEDGMENTS

This work was supported by the Consiglio Nazionale delle Ricerche under U.S.—Italy Cooperative Program Grant No. 47923. The authors would like to thank Professor J. J. Leventhal and Professor T. Woodruff for a critical reading of the manuscript, Mr. M. Badalassi for the preparation of the glass cells, and Mr. F. Papucci for technical assistance.

[1]G. H. Bearman and J. J. Leventhal, Phys. Rev. Lett. **41**, 1227 (1978).

[2]K. S. Kushawaha and J. J. Leventhal, Phys. Rev. A **22**, 2468 (1980).

[3]M. Allegrini, C. Gabbanini, and L. Moi, J. Phys. (Paris) Colloq. **46**, C1-61 (1985).

[4]J. Huennekens and A. Galagher, Phys. Rev. A **27**, 771 (1983).

[5]M. Allegrini, P. Bicchi, and L. Moi, Phys. Rev. A **28**, 1338 (1983).

[6]P. Kowalczyk, Chem. Phys. Lett. **68**, 203 (1979); **74**, 80 (1980); J. Phys. B **17**, 817 (1984).

[7]See, for example, J. B. Hasted, *Physics of Atomic Collisions* (Butterworths, London, 1982).

[8]A. N. Nesmeyanov, *Vapor Pressure of the Chemical Elements* (Elsevier, Amsterdam, 1963).

[9]W. L. Wiese, M. W. Smith, and B. M. Miles, *Atomic Transition Probabilities,* Natl. Bur. Stand. Ref. Data Ser., Natl. Bur. Stand. (U.S.) Circ. No. 22 (U.S. GPO, Washington, D.C., 1969), p. 4.

[10]M. Allegrini, G. Alzetta, K. Kopystyńska, L. Moi, and G. Orriols, Opt. Commun. **19**, 96 (1976); **22**, 329 (1977).

[11]P. Cremaschi, G. Morosi, M. Raimondi, and M. Simonetta, Mol. Phys. **34**, 1483 (1979).

[12]P.-O. Löwdin, J. Chem. Phys. **18**, 365 (1950).

[13]J. Laing and T. F. George, Phys. Rev. A **16**, 1082 (1977).

[14]W. H. Miller and T. F. George, J. Chem. Phys. **56**, 5637 (1972).

[15]A. M. Chang and D. E. Pritchard, J. Chem. Phys. **70**, 4524 (1979).